Anglesite ($PbSO_4$) epitactic overgrowths and substrate-induced twinning on anhydrite ($CaSO_4$) cleavage surfaces

Juan Morales [a], José Manuel Astilleros [a,b,n], Lurdes Fernández-Díaz [a,b], Pedro Álvarez-Lloret [c], Amalia Jiménez [c]

[a] Departamento de Cristalografía y Mineralogía, Universidad Complutense de Madrid, C/ José Antonio Novais 2, Madrid 28040, Spain
[b] Instituto de Geosciencias (CSIC, UCM), C/ José Antonio Novais 2, Madrid 28040, Spain
[c] Departamento de Geología, Universidad de Oviedo, C/Jesús Arias de Velasco, s/n, Oviedo 3305, Spain

A B S T R A C T

The dissolution – precipitation reactions occurring on mineral surfaces are considered an effective means to remove high amounts of dissolved toxic metals from fluid phases by precipitation of a new solid in whose structures the pollutant is immobilized. However, for these reactions to be effi cient a continuous communication between the fluid and mineral phases is required. This communication can be signifi cantly hindered when the new solid phase forms a continuous, homogeneous layer on the mineral substrate. The formation of such a layer is more likely to occur when epitactic relationships exist between the newly formed phase and the mineral substrate. Dissolved lead can be removed by interaction of the Pb-bearing aqueous solution with anhydrite ($CaSO_4$) leading to the formation of anglesite ($PbSO_4$). Here, the relationship between anglesite crystals and an anhydrite substrate is investigated. The three main anhydrite cleavage surfaces, (100), (010), and (001) are considered. A high density of oriented anglesite crystals growing with their (210) plane parallel to the substrate was observed on $(001)_{Anh}$. The density of oriented anglesite was, however, significantly lower on $(100)_{Anh}$ and almost negligible on $(010)_{Anh}$. Anglesite grew with its (001) plane parallel to the substrate on $(100)_{Anh}$, but no evident epitactic relationship was found with $(010)_{Anh}$. Differences in anglesite crystal density are explained on the grounds of structural similarities and the goodness of anglesite – anhydrite matching through the interface. Both on anhydrite (100) and (001) anglesite crystals show at least two specific orientations, which relate to each other through symmetry operators present in the substrate. The coalescence of differently oriented anglesite crystals leads to the formation of twins. This twinning phenomenon is designated as substrate-induced twinning, since the twinning law is determined by the substrate symmetry. In the particular case of anglesite growing on anhydrite (100) two different orientations have been observed, related each other through $(210)_{Ang}$ which act as twin plane.

Keywords: Crystal morphology ; Surface processes; Twinning; Growth from solutions; Epitactic growth; Mineral

1. Introduction

Dissolution–reprecipitation reactions are important for a variety of phenomena, ranging from the development of solvent mediated polymorphic transformations to mineral replacement and fossilization [1–4]. In recent y ears, di ssolution –reprec ipitatio n re actions have been envisaged as a means to remove dissolved pollutants from the environment through their incorporation in the crystal structure of a solid phase [5,6]. The efficiency of such a process mainly depends on the reactivity of the dissolving phase, which releases to the fluid medium the elements with which the pollutant will react, and on the chemical stability of the newly-formed solid [7]. Dissolution–recrystallization reactions often involve the nucleation of the phase that precipitates on a dissolving substrate. When this is the case, the progress of the dissolution–reprecipitation reaction is controlled by the development of a connected porosity netw ork th at guarantees the contact between the reactant solution and the substrate [6,8,9]. Such connectivity can be strongly affected by the existence or absence of epitactic relationships between substrate and overgrowth because an epitactic overgrowth can armor the dissolving substrate from further contact with the solution. Therefore, the efficiency of dissolution–reprecipitation reactions in the removal of pollutants can be strongly affected by the existence of crystallographic relationships between the solid phases involved in the reaction [10,11].

Pb dissolved in natural waters can be removed from the environment via interaction of Pb-bearing solutions with anhydrite

[n] Corresponding author at: Departamento de Cristalografía y Mineralogía, Universidad Complutense de Madrid, C/ José Antonio Novais 2, Madrid 28040, Spain. Tel.: +34 913944881.

E-mail address: jmastill@ucm.es (J.M. Astilleros).

($CaSO_4$) (K_{sp}¼$10^{-4.36}$) and formation of highly insoluble anglesite ($PbSO_4$) (K_{sp}¼$10^{-7.79}$) [12] at ambient conditions. Anhydrite and anglesite are sulfates with different although related structures. The structural similarities of these phases point to the possibility that epitactic relationships can exist between them. Both anhydrite and anglesite crystallize in the orthorhombic system and their struc-tures are based on chains of alternating edge-sharing (SO_4) tetra-hedra and [n]-coordination polyhedra that are linked into a framework. However, whereas in the anhydrite structure divalent Ca is coordinated by eight anions (CaO_8) to form a dodecahedron, in the anglesite structure, Pb cations form an irregular [12]-coordina-tion polyhedron. As a consequence, anhydrite shows Amma sym-metry, with a¼6.993 Å, b¼6.995 Å and c¼6.245 Å [13] whereas anglesite has a barite-type symmetry (Pnma), with a¼8.478 Å, b¼5.397 Å and c¼6.958 Å [14]. On the other hand, the similarity between the a and b cell parameters of anhydrite with the c cell parameter in anglesite might favor the development of epitactic growth and related phenomena. The main objective of this work is, therefore, to explore the characteristics of the overgrowth of anglesite crystals onto anhydrite substrate and, if epitactic relations are found, to interpret them on the base of the structural simila-rities between these phases. This study is focused on the three most frequent surfaces in the habit of natural anhydrite crystals, (100),(001), and (010) [15], which are also those with the lowest attachment energies (E_{att}) [16].

2. Materials and methods

The anhydrite specimens used in all experiments were highly pure (X-ray fluorescence spectroscopic analysis of these crystals revealed that they contained less than 0.4 wt% impurities, with Sr as the main impurity), slightly blue crystals from Naica (Mexico). Prior to the experiments, the crystals were cleaved parallel to (100), (001), and (010) faces with a knife edge to obtain fragments of approximately $3 \times 3 \times 1$ m m ^{3}. The orientation of the sections was unequivocally determined by observing the interference figures in polarized light microscopy. The parent aqueous solutions were prepared using reagent-grade $Pb(NO_3)_2$ and high-purity deionized water (18 MΩ cm) to yield a $[Pb]_{aq}$¼1000 mg/L. Experi-ments were carried out by submerging the cleaved crystals into 5-ml volumes of Pb-bearing aqueous solutions. In order to ensure an optimal interaction with the aqueous solution, the faces with the most exposed area were placed upwards. Anhydrite crystals were removed from the solutions after 2 h of interaction. In all cases, crystals were rapidly dried by blowing pressurized air on their surfaces. All the experiments were carried out at 25 1C and atmospheric pressure.

The samples obtained by the procedure described above were studied by standard scanning electron microscopy (SEM) (JEOL JSM 6400, 40 kV). SEM imaging of the anhydrite surfaces provided information about morphological features of the overgrowths and their crystallographic relationships with the anhydrite surfaces. Energy-dispersive X-ray spectroscopy (EDX) analyses were carried out on selected areas of the samples. The phase(s) resulting from the crystal–solution interaction were identified by Glancing Inci-dence X-ray diffraction (GIXRD), using a Philips X'Pert PRO MRD diffractometer equipped with a Cu Kα source (45 kV, 40 mA) and an angle of incidence of 0.11. The surfaces were scanned over the range 2θ¼20–901 at a scan speed of 0.8 1/min.

In addition, bidimensional X-Ray diffraction analyses were performed to establish the three-dimensional orientation between anhydrite and anglesite overgrowths using an X-ray single crystal diffractometer equipped with a CCD area detector (D8 SMART APEX, Bruker, Germany). For the diffraction experiments, working conditions were: Mo Kα (λ¼0.7093 Å), 50 kV and 30 mA. A set of

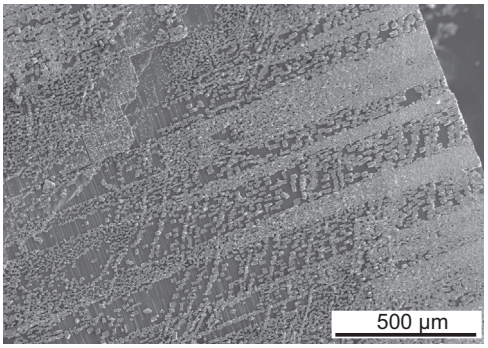

Fig. 1. SEM image obtained after 2 h of exposure of an anhydrite (001) surface to a $[Pb]_{aq}$¼1000 mg/L solution. The anhydrite surface is covered by a discontinuous layer of small anglesite crystals specifically oriented with respect to the substrate.

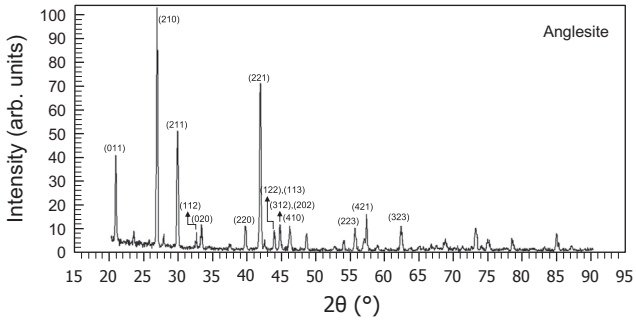

Fig. 2. Glancing Incidence X-Ray diffraction pattern (0.11) recorded after 2 h of reaction at 25 1C on anhydrite (001) cleavage surface in contact with $[Pb]_{aq}$¼ 1000 mg/L. GIXRD pattern confirmed the precipitation of anglesite.

2D diffraction patterns was registered by reflection mode (dif-fractometer ω and 2θ angles were set at 101 and 201 respectively) while rotating the sample around Φ angle (a frame every 51 was registered) with a pin-hole collimator of 0.5 mm in diameter, and an exposure time of 20 s per frame. Pole densities/figures for the main anglesite and anhydrite cleavage surface were calculated from the registered frames using XRD2DScan software [17].

3. Results

The SEM images obtained after 2 h of exposure of the anhydrite (100), (001), and (010) surfaces to the $Pb(NO_3)_2$ solutions show that a mineral–aqueous solution reaction always occurs, irrespec-tive of the interacting surface considered. As a result of this reaction, a more or less discontinuous layer composed of oriented euhedral microcrystals forms on the anhydrite substrate (Fig. 1). EDX analyses of the newly-formed crystals showed that they are composed of S, O and Pb. This composition is consistent with anglesite. The GIXRD analysis also confirmed the formation of anglesite on the surface of anhydrite substrates (Fig. 2). The formation of anglesite occurs through a rapid reaction of Pb^{2+} cations with the SO_4^{2-} ions from the dissolution of anhydrite:

$$CaSO_4 + nH_2O_{(l)} \rightarrow Ca^{2+}_{(aq)} + SO_{4(aq)}^{2-} + nH_2O_{(l)} \quad (1)$$

$$SO_4^{2-}{}_{(aq)} + Pb^{2}{}_{(aq)}{}^{+} \text{-} PbSO_{4(s)} \quad (2)$$

SEM observations reveal that the microscopic features of the anglesite overgrowths largely depend on the anhydrite substrate considered. Differences concern both the orientation and the density of anglesite crystals. In the following subsections the nucleation density of anglesite crystals and their morphology, orientation and twinning will be described separately for each

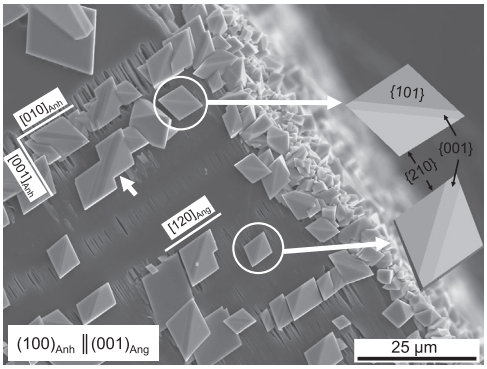

Fig. 3. SEM image of anglesite crystals grown specifically oriented on the (100) surface of an anhydrite cleavage fragment. The epitaxy involves a matching of the plane (100) of anhydrite with the plane (001) of anglesite. The encircled crystals show the two alternative orientations of anglesite on the anhydrite substrate. Both orientations are related to each other by symmetry planes in the anhydrite structure normal to (100). The habit of these crystals is often a combination of the pinacoid {001}, and the rhombic prims {210} and {101} as shown in the drawings. The short white arrow points out the coalescence of equally oriented anglesite crystals, which leads to the formation of short arrow-like habits.

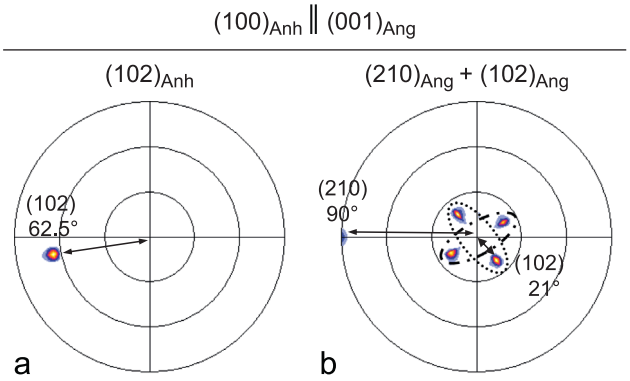

Fig. 4. Poles figures (PF) obtained from 2DXRD patterns showing the crystal-logra phic orientation relationships between anhydrite cleavage surfaces and over-growth of anglesite crystals: $(100)_{Anh}\|(001)_{Ang}$. Pole figure centers indicate (100) anhydrite and (001) anglesite maxima respectively (not shown). Angular tilt values from pole figure center are represented by arrows. (a) PF for (102) anhydrite displaying a defined maximum at a tilt of 62.51 from the center of the figure, corresponding to the orientation of the (100) anhydrite cleavage surface. (b) PFs for (210) and (102) anglesite crystals tilted by 901 and 211 respectively from the center of the figure, corresponding to (001) anglesite crystal plane orientation. Two sets of (102) anglesite crystals orientation are represented by elipse dots/lines.

orientation of the anhydrite substrates, (100), (001), and (010). The features of the anglesite overgrowth point to a clear crystal-logra phic control being exerted by the anhydrite substrate. The characteristics of this control are discussed in Section 4.

3.1. Anglesite overgrowth on anhydrite (100)

The SEM images obtained after 2 h of exposure of the anhydrite (100) surface to the $Pb(NO_3)_2$ solutions reveal the substrate to be partially covered by anglesite crystals. A detailed view of this overgrowth is shown in Fig. 3. Due to its very good cleavage, anhydrite (100) surfaces usually consist of very flat, large terraces bounded by macrosteps. The interaction of such a surface with an aqueous solution undersaturated with respect to anhydrite leads to a partial dissolution of the terraces by the formation and spread of deep etch pits. These etch pits usually show a typical pencil shape elongated along [001] which enables the identification of the main crystallographic directions on this surface [18]. The anglesite overgrowth is composed of small (10–20 mm) rhombus-shaped crystals which are clearly oriented with respect to the substrate. Moreover, these crystals preferentially form in the proximity to the etch pits on the anhydrite surface. The prevailing habit of these crystals is a combination of the pinacoid {001}, and the rhombic prims {210} and {101}. The corresponding crystal faces are indicated in Fig. 3. However, {001} and {101} do not always coexist in the same crystal. All these forms occur frequently in natural anglesite crystals [15].

The anglesite crystals are clearly oriented with respect to the substrate. The epitaxy involves a matching between the planes (100) of anhydrite and (001) of anglesite: $(100)_{Anh}\|(001)_{Ang}$. Moreover, it becomes apparent that ⟨120⟩ edges of anglesite, resulting from the intersection of {210} with {001} forms, run parallel to the [010] direction of the anhydrite substrate.

In addition, preferential orientation of the anglesite crystals overgrowth in relation to the (100) anhydrite cleavage surface was further characterized by the determination of pole figures obtained by 2DXRD analyses. In order to define the (100) anhydrite cleavage surface orientation, the pole figure for the (102) reflection was determined, showing a maximum tilted by 62.51 with respect to the pole figure center which coincides with (100) anhydrite cleavage surface (Fig. 4a). On the other hand, a pole figure for combined (210) and (102) reflections for anglesite crystals grown on anhydrite (100) displays a maximum tilted by 901 for the (210) reflection and a set of four maxima for the (102) pole figure titled by 211 from the center which in this case corresponds to the (001) plane of anglesite crystals (Fig. 4b). Pole figures for anhydrite (100) and anglesite (001) cannot be shown due to their similar d-spacing. The set of different orientations for the (102) pole figure is the result of anglesite crystals with two alternative orientations related by a rotation by 901 on the anhydrite (100) surface (see Fig. 3). Both orientations are statistically equivalent since they are related one to each other by symmetry operators inherent to the anhydrite structure normal to the (100) substrate plane. The nucleation of anglesite crystals on the anhydrite substrate with such different and symmetry related orientations leads to the formation of induced twins [19] where differently oriented anglesite crystals coalesce as a result of growth. An example of this so called induced twinning is shown in Fig. 5a,b, where the two alternative orientations of anglesite crystals can be observed at a high magnification. On the other hand, the coalescence of equally oriented anglesite crystals leads to the formation of larger single crystals. This second type of coalescence explains the formation of typical short arrow-like crystals [20], as shown in Fig. 3.

3.2. Anglesite overgrowth on anhydrite (001)

After the interaction period, the anhydrite (001) substrates were partially covered by anglesite crystals of about 20 mm i n length (Fig. 6). Also in this case, anglesite crystals clearly show preferred orientations with respect to this substrate. On average, the density of anglesite crystals formed on this surface is sig-nificantly higher than on anhydrite (100) and (010) substrates. Although the anglesite overgrowth forms a coating that totally covers large areas of the (001) anhydrite substrate, this coating is irregular, leaving some areas free of crystals. In such cleared areas the typical grooves regularly oriented parallel to [100] were observed which, again, enabled defining the main crystallo-graphic directions on this anhydrite surface [21]. The habit of the anglesite crystals formed on this surface result from a combination of {001}, {210} and {101} forms more or less developed, similarly as occurs on anhydrite (100). In this case, the epitaxy is defined by a matching of the plane (001) of anhydrite with the (210) planes (or their equivalent ones) of anglesite: $(001)_{Anh}\|(210)_{Ang}$ (Fig. 6). The long [120] edges of anglesite crystals, defined by the inter-section of {210} and {001} forms, are oriented parallel to [010] of

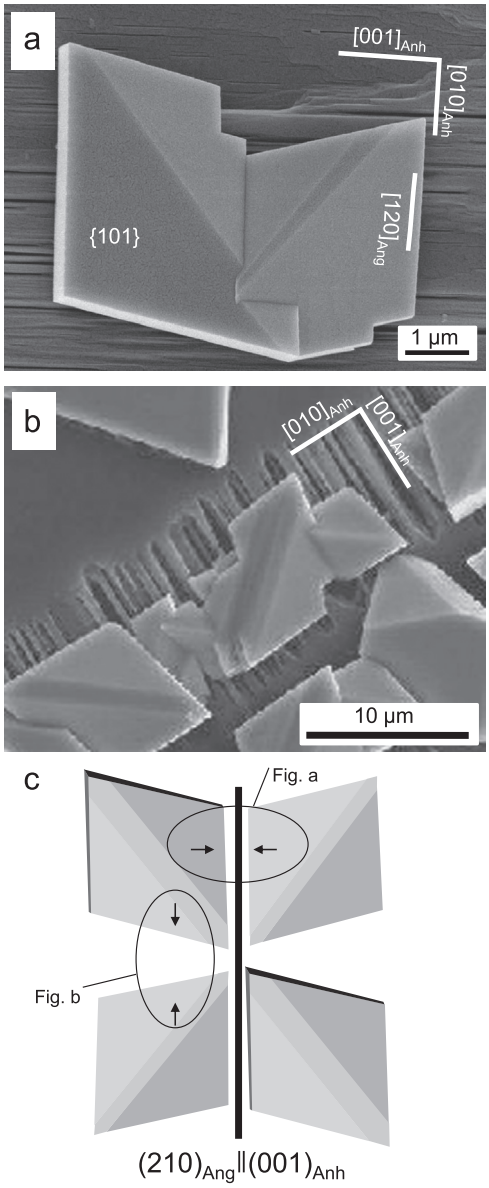

Fig. 5. SEM images of substrate-induced anglesite twins grown on an anhydrite (100) surface. This phenomenon occurs when two neighbored anglesite crystals with different epitactic orientations (a) and (b) coalesce while they grow. The relative orientations of the two parts of the intergrowths can be easily related each other through $(210)_{Ang}$ (parallel to $(001)_{Anh}$) which act as twin plane (c). The sketch (c) shows how the coalescence of individuals can occur differently.

the anhydrite substrate, while the shorter [001] edges of anglesite, defined by the intersection of the faces of the {210} form, are parallel to [100] of the anhydrite substrate. As in the previous case, this crystallographic orientation relationship is also confirmed from the determination of pole figures for anhydrite cleavage surface and overgrown anglesite crystals. The pole figure for $(200)_{Anh}$ reflection (Fig. 7a) shows a maximum tilted 901 from center, that represents (001) anhydrite cleavage surface orienta-tion. Moreover, the pole figure for the combined (101) and (200) anglesite crystals reflections (Fig. 7b) displays two maxima tilted 581 and 401, respectively, from the center of the pole figure, that indicates the (210) anglesite crystal orientation. Pole figures for (001) of anhydrite and (210) of anglesite are not represented due to their similar d-spacing.

Here, it is also easy to establish relationships between the main directions of the substrate and the overgrowth since the elongation direction in anglesite crystals, $[120]_{Ang}$, runs parallel to either $[100]_{Anh}$ or $[010]_{Anh}$. These two alternative orientations define the following relationships: (1) $[010]_{Anh}\|$ $[1\ 2\ 0]_{Ang}$, $[\ 1\ 0\ 0\ ]_{Anh}\|[001]_{Ang}$ and (2) $[010]_{Anh}\|[001]_{Ang}$, $[\ 1\ 0\ 0\ ]_{Anh}\|[120]_{Ang}$. It is worth to note that these two main alternative crystal orientations are not symmetrically equivalent because they are not related by any symmetry operator of the substrate. Moreover, both orientations are neither statistically equivalent since the density of anglesite crystals oriented with their elongation direction $[120]_{Ang}$ parallel to $[010]_{Anh}$ is much higher. Finally, the existence of (100) and (010) mirror planes in the anhydrite structure determines, in turn, the existence of two statistically equivalent orientations of anglesite crystals with respect to the anhydrite substrate for each one of the two alternative epitactic relationships defined above. In short there are four different orientations of anglesite crystals on the anhydrite substrate which are symmetrically related two by two.

3.3. Anglesite overgrowth on anhydrite (010)

The inspection with SEM shows that the density of anglesite crystals formed on anhydrite (010) surface is smaller than the observed on (100) and (001) substrates. Moreover, on this particular surface anglesite crystals are not equally spaced but preferentially nucleated on cleavage macrosteps and on steps bounding etch pits elongated along [001] (Fig. 8). In contrast, anglesite crystals growing on terraces are very scarce. Crystals related to macrosteps are bigger and exhibit well-developed flat faces, with their habit defined by a combination of {001}, {210} and/or {101} forms, with the pinacoid {010} as minor form in some of them. It is also worthwhile to note that anglesite crystals formed on straight [001] steps of anhydrite are scarce, while a much higher density of these crystals nucleated on the rougher [100] steps resulting from the coalescence of etch pits. These observations point to a bad matching between anglesite and anhydrite on this particular surface. Moreover, the high concentration of anglesite crystals on [100] steps seems to indicate that here anglesite does not nucleate on the anhydrite (010) face but on anhydrite (001) substrates exposed at [100] steps. In fact, the anglesite crystals observed on [100] steps show identical characteristics to those directly observed on (001) surfaces. The small number of anglesite crystals which appear distributed on terraces at random orientations most likely correspond to crystals detached during the handling of the sample and settled on the (010) anhydrite substrate. The low density of anglesite crystals on this anhydrite cleavage surface does not allow the determination of orientation relationship with anglesite crystals by means of 2DXRD analyses.

4. Discussion

4.1. Anglesite habit

Crystal habits result from a complex interplay between struc-ture and external factors affecting the crystal growth process. The final habit of the anglesite single crystals grown onto the anhydrite surfaces is defined by a combination of {210}, {001}, and {101} forms, with {210} faces appearing on all anglesite crystals, whereas {101} or {001} can be eventually absent. On a few anglesite crystals {010} form has also been observed. According to the theory of Hartman and Perdok [22], it is possible to assess the character of any {hkl} form of a crystal by analyzing the PBCs (periodic and uninterrupted bond chains in a given crystal structure): two PBCs determine a layer of strong bonds parallel to some (hkl) face. Faces limiting such layers (F for flat) are more stable than those parallel to one (S¼stepped) or none (K¼kinked) PBC. Hartman and Strom [23] applied the PBC analysis to a barite type structure, defining {210}, {001}, and {101}, along with {211}, and {201} as the faces

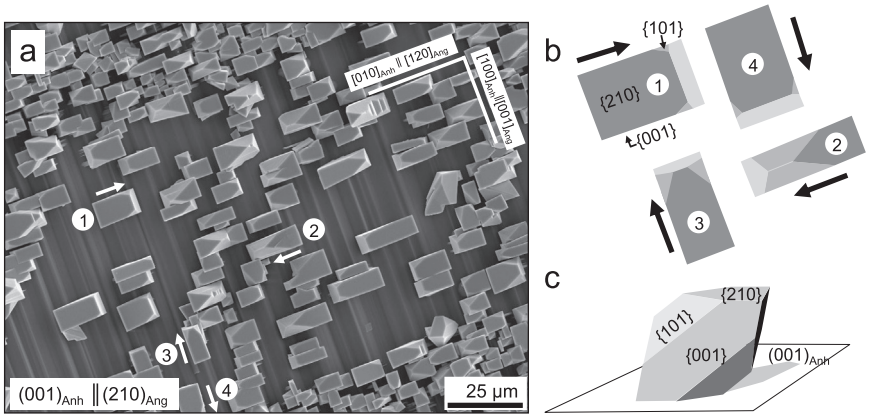

Fig. 6. (a) SEM image showing the epitactic growth of anglesite crystals on an anhydrite (001) surface. The epitaxy is defined by $(001)_{Anh}\|(210)_{Ang}$. (b) There are four different orientations of anglesite crystals on the anhydrite substrate which are symmetrically related two by two. (c) Simulation of the typical morphology of the crystal in these experiments.

that have an F-character. The theoretical habit of a crystal can be built by considering the growth rate of F faces as proportional to their attachment energy (E_{att}). Calculated attachment energies (E_{att}) for the aforementioned F faces predict a theoretical habit for barite type crystals dominated by {210}, {001} and {101} faces. The morphology of the anglesite crystals formed on anhydrite (100), (010) and (001) surfaces is also bounded by the {210}, {001} and {101} faces in agreement with this prediction. Moreover, it is also very close to the habit proposed for barite crystals grown under low supersaturation conditions [24]. Although an estima-tion of supersaturation during the growth of anglesite on anhy-drite is beyond the scope of this work, the close similarity of anglesite crystal habits to that predicted by PBC theory for barite type crystals points to anglesite growth occurring under low supersaturation conditions or a limited influence of this external factor on the growth morphology of anglesite. It is worth to note that the dissolution of anhydrite, which provides a continuous source of sulfate ions, guaranteeing the progress of anglesite growth, also releases Ca^{2+} ions to the growth medium. The concentration of this ion progressively increases with time. However, no significant disruption of the anglesite crystal habits has been observed that can be related to the presence of Ca in the growth medium.

Finally, it is interesting to highlight the influence exerted by the epitactic relationships between the substrate and the overgrowth on the morphology of anglesite crystals. Although their habit is bounded by {210}, {100} and {101} faces in all the cases, the relative importance of such faces varies depending on the anhy-drite substrate on which anglesite crystals develop. Thus, the comparison of images in Figs. 3 and 6 shows that while {101} is the most important form in the habit of anglesite formed on anhydrite (100), this form is much less developed or even absent in anglesite crystals grown on anhydrite (001), which show a morphology dominated by {210} and {001}. This could be explained as a result of a better matching of between $\{210\}_{Ang}$ and $\{001\}_{Anh}$ than between $\{001\}_{Ang}$ and $\{100\}_{Anh}$. Such better matching could also explain the anisotropic development of equivalent faces belonging to the {210} form, with the faces parallel to the $(001)_{Anh}$ substrate being more developed.

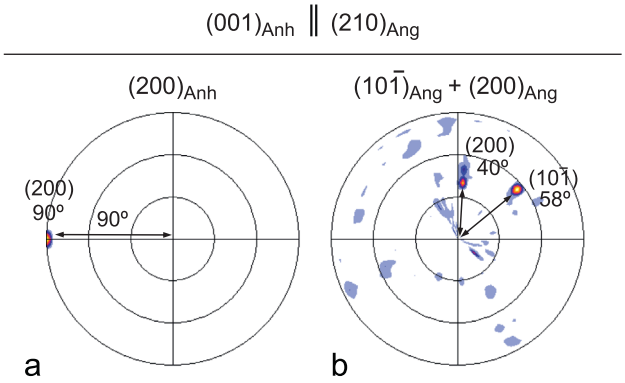

Fig. 7. Poles figures (PF) obtained from 2DXRD patterns showing the crystallographic orientation relationships between anhydrite cleavage surfaces and overgrowth of anglesite crystals: $(001)_{Anh}\|(210)_{Ang}$. Pole figure centers indicate (001) anhydrite and (210) anglesite maxima respectively (not shown). Angular tilt values from pole figure center are represented by arrows. (a) PF for (200) anhydrite displaying a defined maximum tilted by 901 from the center of the figure indicating (001) anhydrite cleavage surface orientation. (b) PFs for (011) and (200) anglesite crystals tilted by 581 and 401 respectively from the center of the figure indicating (210) anglesite crystals orientation.

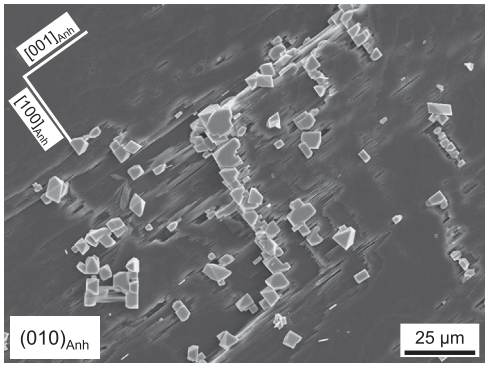

Fig. 8. SEM images on anhydrite (010) surfaces showing the anglesite crystals preferentially arranged along [100] on anhydrite macrosteps resulting from the dissolution of cleaved steps and etch pits.

4.2. Anhydrite and anglesite: epitactic relationships, nucleation density and induced twinning

In order to understand the development of an epitaxy, the structural matching between the overgrowth and the substrate must be considered. This requires a comparison of geometrical features of the crystal lattices of both phases as well as the structural elements that they share. In the anhydrite structure, Ca^{2+} is coordinated to eight oxygen atoms belonging to six different SO_4^{2-} tetrahedra. As a result, sulfate–calcium chains can be distinguished. The PBC analysis of anhydrite structure [16] reveals three elementary sulfate–calcium–sulfate bond chains which run parallel to the main crystallographic axes. These PBCs

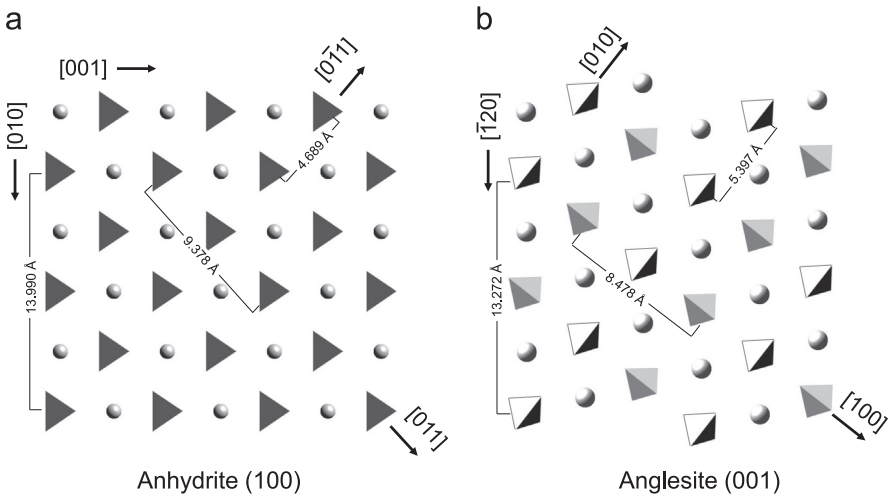

Fig. 9. Projections of the crystal structures of (a) a (200) slice of anhydrite and (b) a (002) slice of anglesite.

Table 1
Epitactic relationships between anhydrite ($CaSO_4$) and anglesite ($PbSO_4$).

Anhydrite ($CaSO_4$)		Anglesite ($PbSO_4$)		Misfit (%)	
Contact Plane	Parameter (Å)	Contact plane	Parameter (Å)	Linear	Angular
(100)	$2\times[010]=13.990$	(001)	$\langle 120\rangle=13.772$	−1.92	
	$\langle 011\rangle=4.689$		$[010]=5.397$	15.10	3.63°
	$2\times\langle 011\rangle=9.378$		$[100]=8.478$	−9.66	10.10°
(001)	$[100]=6.993$	(210)	$[001]=6.955$	−0.54	
	$2\times[010]=13.990$		$\langle 120\rangle=13.772$	−1.92	
	$[010]=6.995$		$[001]=6.955$	−0.57	
	$2\times[100]=13.986$		$\langle 120\rangle=13.772$	−1.89	

provide an F-character to the three anhydrite surfaces considered in this study, $\{100\}_{Anh}$, $\{0\ 1\ 0\}_{Anh}$, and $\{001\}_{Anh}$. In the anglesite structure, at least ten PBCs have been found [23]. Among them, those parallel to $[001]_{Ang}$ and $\langle 120\rangle_{Ang}$ are most stable and consist of a sequence of Pb-sulfate bonds, which is linear along $\langle 120\rangle_{Ang}$ and arranged in a zig–zag chain along $[001]_{Ang}$. As explained above, the epitactic growth of anglesite on anhydrite is controlled by the parallelism between these two directions in anglesite and $[100]_{Anh}$ and $[010]_{Anh}$. The fact that the directions involved in both the substrate and the overgrowth are PBCs composed of cation–sulfate bonds explains the structural affinity between both minerals.

Fig. 9 displays a comparison between the projections of the structures of anhydrite (100) and anglesite (001) faces which are the contact planes in the epitaxy described in Section 3.1. Both structures are projected in the same orientation as shown in the SEM images (Figs. 3 and 5), with the $[120]_{Ang}$ running parallel to the $[010]_{Anh}$. For anhydrite, the distance between successive SO_4 groups along [010] is 6.995 Å, i.e., it coincides with the b cell parameter. In the anglesite structure, the distance between successive equivalent SO_4 groups (repeating period) is 13.772 Å, which is about twice the distance between successive SO_4 groups along $[010]_{Anh}$ (2 × 6.995 Å¼13.990 Å). Similar repeating periods mean good matching between the two structures. The mismatch can be described by the lattice misfit (mf), which is frequently expressed using the equation [25]:

$$mf(\%)=\frac{t_{[uvw]_{Ang}}-t_{[uvw]_{Anh}}}{t_{[uvw]_{Anh}}}100 \qquad (3)$$

where $t_{[uvw]}$ is the repeating period along the [uvw] direction in the substrate (anhydrite) and overgrowth (anglesite). Negative misfit values mean that the unit cell of the overgrowth is contracted along [*uvw*] in comparison to the unit cell of the substrate ($t_{[uvw]_{Ang}} < t_{[uvw]_{Anh}}$). Considering a 1:2 ratio between the repeating periods along $[010]_{Anh}$ and $\langle 120\rangle_{Ang}$, the misfit is only −1.92% (Table 1). This misfit is clearly within the limits required for epitactic nucleation from solution, which justifies the development of an oriented overgrowth of anglesite on the anhydrite (100) surface. Although less obvious, there are also two additional pairs of directions lying within the contact plane, $\langle 011\rangle_{Anh}\|[010]_{Ang}$ and $2\times\langle 011\rangle_{Anh}\|[100]_{Ang}$. These pairs show relatively low divergences in the repeating periods (see Table 1) and their linear misfits (mf=15.10% and −9.66%, correspondingly) could be considered within the limits to promote epitactic growth. However they also show angular divergences (3.63° and 10.11°, correspondingly) which do not favor the development of epitaxy.

The matching between the two structures through the $(001)_{Anh}$ and $(210)_{Ang}$ (i.e., the contact planes between both structures as described in Section 3.2 and showed in Fig. 6) is even better (Table 1). Fig. 10 shows the projections of the structures of anhydrite and anglesite on (001) and (210), respectively. These projections show $\langle 120\rangle_{Ang}$ running parallel to the $[010]_{Anh}$. A s explained above, the linear misfit between them is −1.92%. How-ever, the matching is significantly better between $[100]_{Anh}$ and $[001]_{Ang}$. The repeating period along these directions are 6.993 and 6.955 Å, which means a misfit of only −0.54. It appears, therefore, that from a geometric standpoint, this epitaxy can be considered two-dimensional. On the other hand, the fact that a and b axes in anhydrite structure are almost identical in length, enables the exchange of [100] by [010] with little change of the repeating periods (Table 1). As a consequence, the matching between $[010]_{Anh}\|[001]_{Ang}$, and $[100]_{Anh}\|\langle 120\rangle_{Ang}$ are also excel-lent, with misfits of −0.57 and −1.89, respectively. The good matching between the two pair of directions in this second

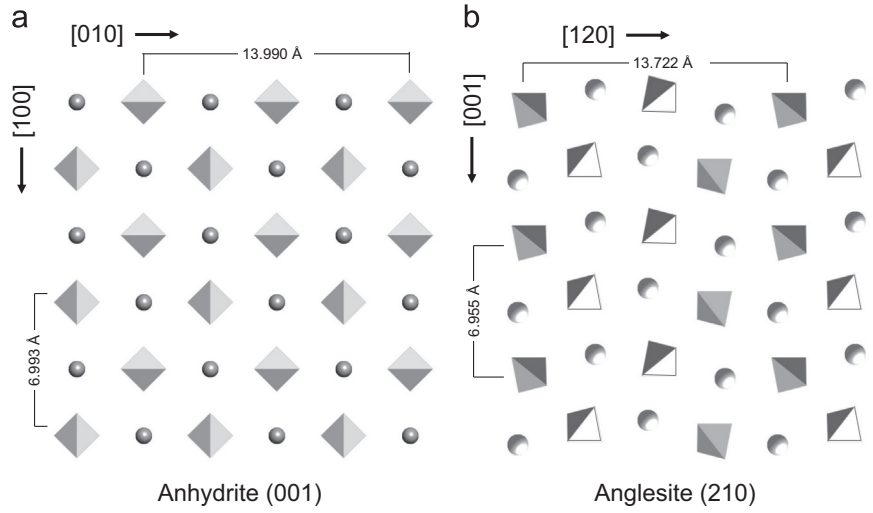

Fig. 10. Projections of the crystal structures of (a) a (002) slice of anhydrite and (b) a (210) slice of anglesite.

orientation explains, therefore, the development of two non-symmetrically related populations of anglesite crystals rotated by 901 with respect to each other. Moreover, a direct consequence of the good matching between the two structures is the existence of a significantly higher density of anglesite crystals on anhydrite (001) surface than on the other two orientations of the substrate considered.

As we have shown at length in the results section, the result of having two or more equiprobable orientations of anglesite on the anhydrite surfaces can lead to the development of the so-called induced twinning [19]. Such a phenomenon has been clearly observed on anhydrite (100) surface (Fig. 5a,b), where the two equiprobable orientations are $[120]_{Ang}\|[010]_{Anh}$ and $[\bar{1}20]_{Ang}\|[010]_{Anh}$. Independently of how the individuals coalesce, both orientations can be easily related to each other through $(210)_{Ang}$ (parallel to $(001)_{Anh}$) which act as twin plane (Fig. 5c).

The anglesite twins observed on anhydrite (100) (Fig. 5a,b) cannot be interpreted as examples of growth twins because they do not develop as a result of the direct nucleation of a crystal individual onto its twinned one. On the contrary, since the formation of these twins is due to the coalescence of individuals differently oriented with respect to the substrate and the twin law is determined by the substrate symmetry, this twinning phenom-enon can be designated as substrate-induced twinning. In the particular case of anglesite growing on an anhydrite (100) surface, the extensive development of twins involving crystals that show the four orientations observed with respect to the substrate could lead to the formation of a tartan-like pattern. Tartan-like twinning is not uncommon in minerals and normally develops as a result of displacive polymorphic transformations, as in the case of micro-cline twinning [26]. However, the examples of substrate-induced twinning described in this work can in no case be considered as examples of transformation twinning, since the fact that their development during a dissolution–precipitation process is merely circumstantial. One can easily envisage the formation of similar twins as a result of direct nucleation and growth of anglesite on an anhydrite (100) substrate in contact with an aqueous solution initially supersaturated with respect to that phase.

5. Conclusions

The experimental results obtained in this research indicate that the interaction of anhydrite surfaces with highly concentrated Pb-aqueous solutions leads to their dissolution coupled to the nucleation of anglesite. The structural similarity between anglesite and anhydrite facilitates the epitactic growth of anglesite on the three main anhydrite cleavage surfaces. Anglesite crystals can show different orientations on specific anhydrite surfaces. These differently oriented anglesite crystals are related to each other via a symmetry operator present in the anhydrite substrate. The coalescence of these crystals leads to the formation of the so-called substrate-induced twinning.

These experimental results also indirectly suggest that the surface of anhydrite is a potential scavenger of dissolved Pb since during the interaction between anhydrite surfaces and highly concentrated Pb-aqueous solutions this heavy metal is continu-ously removed from the contaminated water as the reaction proceeds. However, the epitactic character of anglesite growth on the main anhydrite surfaces could determine that the efficiency of this process was significantly reduced as a result of an early substrate isolation by a layer of oriented overgrowth. Establishing the actual influence of the epitactic relationships between anhy-drite and anglesite on the efficiency of anhydrite surfaces as Pb sorbants requires a specific research and will be the subject of a future work from this laboratory.

Acknowledgments

This research was supported by MICINN-Spain, under grants, CGL2010-20134-C02-01 and CGL2011-25906. J. Morales acknowl-edges a FPI fellowship from the Spanish MICINN. We sincerely thank the Microscopy Centre and the X-ray Diffraction Central Service of the Complutense University (UCM) for technical assis-tance. We appreciate the insightful comments by an anonymous reviewer.

References

[1] P.T. Cardew, R.J. Davey, The kinetics of solvent-mediated phase transformations, Proc. R. Soc. London A 398 (1985) 415–428.
[2] R.E. Martin, Taphonomy: A Process Approach. Cambridge Paleobiology Series, Cambridge University Press, Cambridge, 1999.
[3] A. Putnis, Mineral replacement reactions: from macroscopic observations to microscopic mechanisms, Mineral. Mag. 66 (2002) 689–708.
[4] C.V. Putnis, L. Fernández-Díaz, Ion partitioning and element mobilization during mineral replacement reactions in natural and experimental systems, in: M. Prieto, H. Stoll (Eds.), Ion Partitioning in Ambient-Temperature Aqueous Systems. EMU Notes in Mineralogy 10, European Mineralogical Union and the Mineralogical Society of Great Britain & Ireland, London, 2010, pp. 189–226.

[5] Q.Y. Ma, S.J. Traina, T.J. Logan, J.A. Ryan, In situ lead immobilization by apatite, Environ. Sci. Technol. 27 (1993) 1803–1810.
[6] M. Prieto, P. Cubillas, A. Fernández-González, Uptake of dissolved Cd by biogenic and abiogenic aragonite: a comparison with sorption onto calcite, Geochim. Cosmochim. Acta 67 (2003) 3859–3869.
[7] A. Godelitsas, J.M. Astilleros, Dissolution, sorption/(re)precipitation, formation of solid solutions and crystal growth phenomena on mineral surfaces: implications for the removal of toxic metals from the environment, in: M. Prieto, H. Stoll (Eds.), Ion Partitioning in Ambient-Temperature Aqueous Systems. EMU Notes in Mineralogy 10, European Mineralogical Union and the Mineralogical Society of Great Britain & Ireland, London, 2010, pp. 289–324.
[8] C.V. Putnis, K. Mezger, A mechanism of mineral replacement: isotope tracing in the model system KCl–KBr–H_2O, Geochim. Cosmochim. Acta 68 (2004) 2839–2848.
[9] C.V. Putnis, K. Tsukamoto, Y. Nishimura, Direct observations of pseudomorphism: compositional and textural evolution at a fluid – solid interface, Am. Mineral. 90 (2005) 1909–1912.
[10] J.D. Rodríguez-Blanco, A. Jiménez, M. Prieto, Oriented overgrowth of pharmacolite ($CaHAsO_4 \cdot 2H_2O$) on Gypsum ($CaSO_4 \cdot 2H_2O$), Cryst. Growth Des. 7 (2007) 2756–2763.
[11] C. Pérez-Garrido, L. Fernández-Díaz, C.M. Pina, M. Prieto, In situ AFM observations of the interaction between calcite {1014} surfaces and Cd-bearing aqueous solutions, Surf. Sci. 601 (2007) 5499–5509.
[12] D.L. Parkhurst, C.A.J. Appelo, User's guide to PHREEQC (Version 2)-A computer program for speciation, batch-reaction, one-dimensional transport and inverse geochemical calculations, Water-Resources Investigations Report, US Geological Survey99–4259.
[13] F.C. Hawthorne, R.B. Ferguson, Anhydrous sulphates. II. Refinement of the crystal structure of anhydrite, Can. Mineral. 13 (1975) 289–292.
[14] J. Majzlan, A. Navrotsky, J.M. Neil, Energetics of anhydrite, barite, celestine, and anglesite: a high-temperature and differential scanning calorimetry study, Geochim. Cosmochim. Acta 66 (2002) 1839–1850.
[15] I. Kostov, R.I. Kostov, Crystal habits of minerals. Bulgarian Academic Monographs (1), Pensoft Publishers and Prof. Marin Drinov Academic Publishing House, Sofia, 1999.
[16] D. Aquilano, M. Rubbo, M. Catti, A. Pavese, P. Ugliengo, Theoretical equilibriumand growth morphology of anhydrite ($CaSO_4$) crystals, J. Cryst. Growth (1992)519–532.
[17] A.B. Rodriguez-Navarro, XRD2DScan: new software for polycrystalline materials characterization using two-dimensional X-ray diffraction, J. Appl. Crystallogr 39 (2006) 905–909.
[18] H. Shindo, K. Shitagami, S. Kondo, A. Seo, Atomic force microscope observation of directional growth and dissolution on surfaces of sulphate minerals, J. Cryst. Growth 198/199 (1999) 253–257.
[19] A.J. Pinto, A. Jiménez, M. Prieto, Interaction of phosphate bearing solutions with gypsum: epitaxy and induced twinning of brushite ($CaHPO_4 \cdot 2H_2O$) on the gypsum cleavage surface, Am. Mineral. 94 (2009) 313–322.
[20] N. Sánchez Pastor, C.M. Pina, J.M. Astilleros, L. Fernández-Díaz, A. Putnis,Epitaxial growth of celestine on barite (001) face a molecular scale, Surf. Sci.581 (2–3) (2005) 225–235.
[21] H. Shindo, A. Seo, T. Watabe, Structures of the $CaSO_4$ (001) surface studied with atomic force microscopy in air and in solution, Phys. Chem. Chem. Phys. 2 (2001) 230–234.
[22] P. Hartman, W. Perdok, On the relations between structure and morphology of crystals I, Acta Crystallogr. 8 (1955) 49–52.
[23] P. Hartman, C.S. Strom, Structural morphology of crystals with the barite ($BaSO_4$) structure: a revision and extension, J. Cryst. Growth 97 (1989) 502–512.
[24] M. Prieto, A. Putnis, J. Arribas, L. Fernández-Díaz, Ontogeny of baryte crystals grown in a porous medium, Mineral. Mag. 56 (1992) 587–598.
[25] J.H. van der Merwe, The role of lattice misfit in epitaxy, Crit. Rev. Solid State Mater. Sci. 7 (1978) 209–231.
[26] A. Putnis, Introduction to Mineral Sciences, Cambridge University Press, Cambridge, UK, 1992.